Aberrant expression and subcellular localization of ECT2 drives colorectal cancer progression and growth

Danielle R. Cook[1], Melissa Kang[2], Timothy D. Martin[3], Joseph A. Galanko[2], Gabriela H. Loeza[4], Dimitri G. Trembath[5,6], Verline Justilien[7], Karen A. Pickering[8], David F. Vincent[8], Armin Jarosch[9], Philipp Jurmeister[9], Andrew M. Waters[5], Priya S. Hibshman[5,10], Andrew D. Campbell[8], Catriona A. Ford[8], Temitope O. Keku[2], Jen Jen Yeh[3,5,11], Michael S. Lee[4,5], Adrienne D. Cox[3,5,12], Alan P. Fields[7], Robert S. Sandler[2], Owen J. Sansom[8,13], Christine Sers[9,14,15], Antje Schaefer[3,5 #], and Channing J. Der[1,3,5,9 #]

Figure S1 Cook et al.

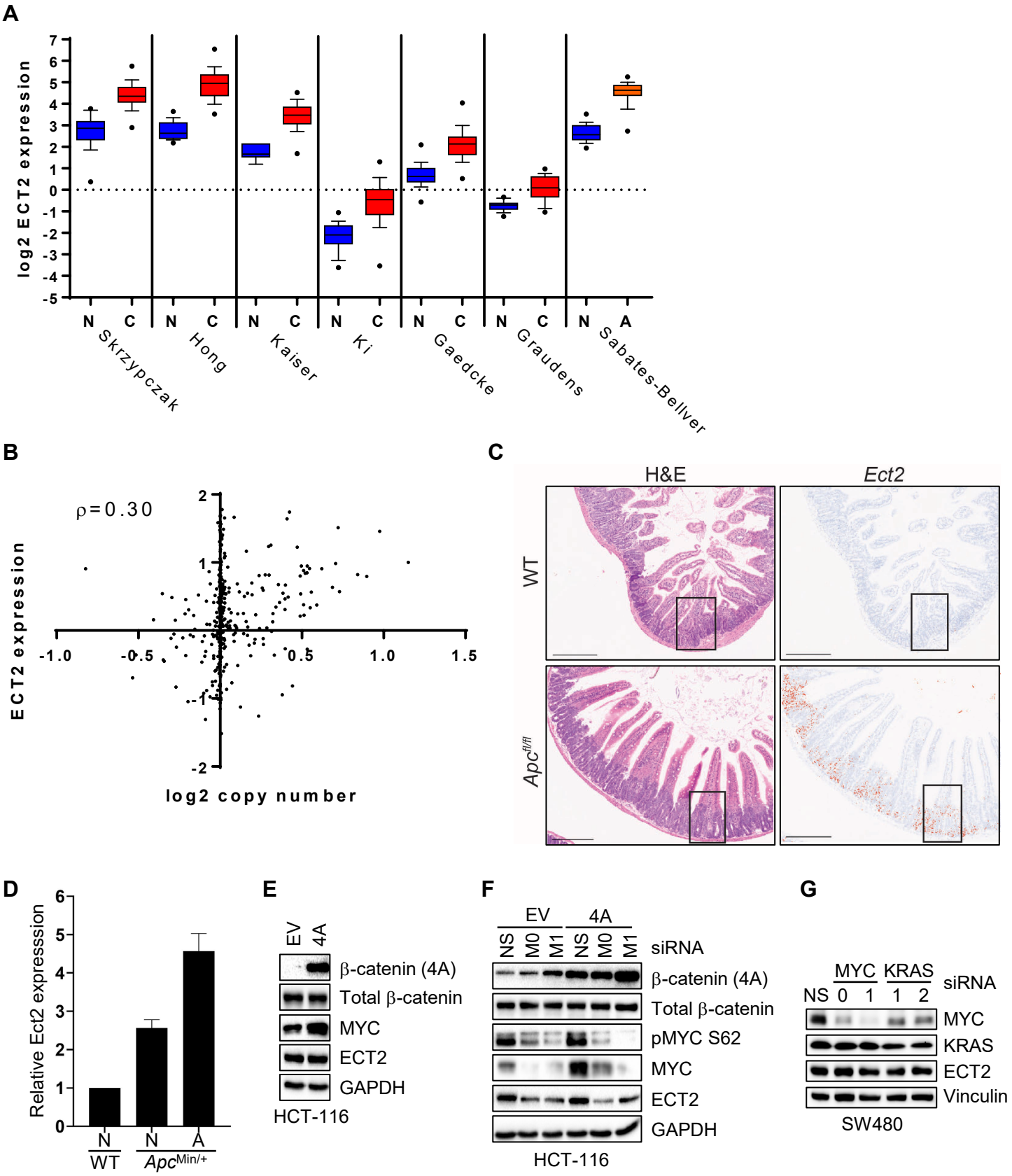

Supplementary Figure S1. Increased *ECT2* mRNA and protein expression in CRC**.** **A**, Comparison of *ECT2* gene expression between normal colorectal tissues (N), colorectal cancers (C), or adenomas (A), based on seven published studies. Gene expression levels were median-centered within each study. The number of samples in each arm is as follow: Skryzpczak, (N 24, C 81) (1); Hong (N 12, C 70) (2), Kaiser (N 5, C 100) (3), Ki (N 41, C 77), Gaedcke (N 65, C 65) (4), Graudens (N 12, C 46) (5), Sabates-Bellver (N 32, A 32) (6). **B**, Spearman correlation between *ECT2* gene expression as determined by RNA-Seq and genomic copy number in 376 CRC samples. Association between ECT2 expression and APC loss. **C**, Representative images of hematoxylin and eosin (H&E) stained or Ect2–specific RNA-ISH (RNAscope) stained tissue specimens from the small intestine of wild-type (*Vil-CreER Apc*$^{+/+}$) and *Vil-CreER Apc*$^{fl/fl}$ mice. Scale bar, 300 μm. Annotations highlight regions shown at higher magnification in Fig. 1H. **D**, Quantitation of ECT2 expression from wild-type (WT) or *Apc*$^{Min/+}$ mouse-derived normal (N) or adenoma (A) tissue, n = 2. Representative immunoblot shown in Fig. 1J. ***E***, Immunoblots of HCT-116 cells ectopically expressing activated β-catenin (4A) or empty vector (EV). **F,** Immunoblots of HCT-116 cells ectopically expressing activated β-catenin (4A) or empty vector (EV), followed by depletion of MYC using two different siRNAs (M0, M1); NS = non-targeting siRNA. Data in **E, F** are representative of three independent experiments. GAPDH was used as loading control. **G**, Immunoblots of SW480 cells treated with two different siRNAs to deplete MYC (0, 1) or KRAS (1, 2). NS = non-targeting siRNA. Vinculin was used as loading control. Data are representative of three independent experiments.

Figure S2 Cook et al.

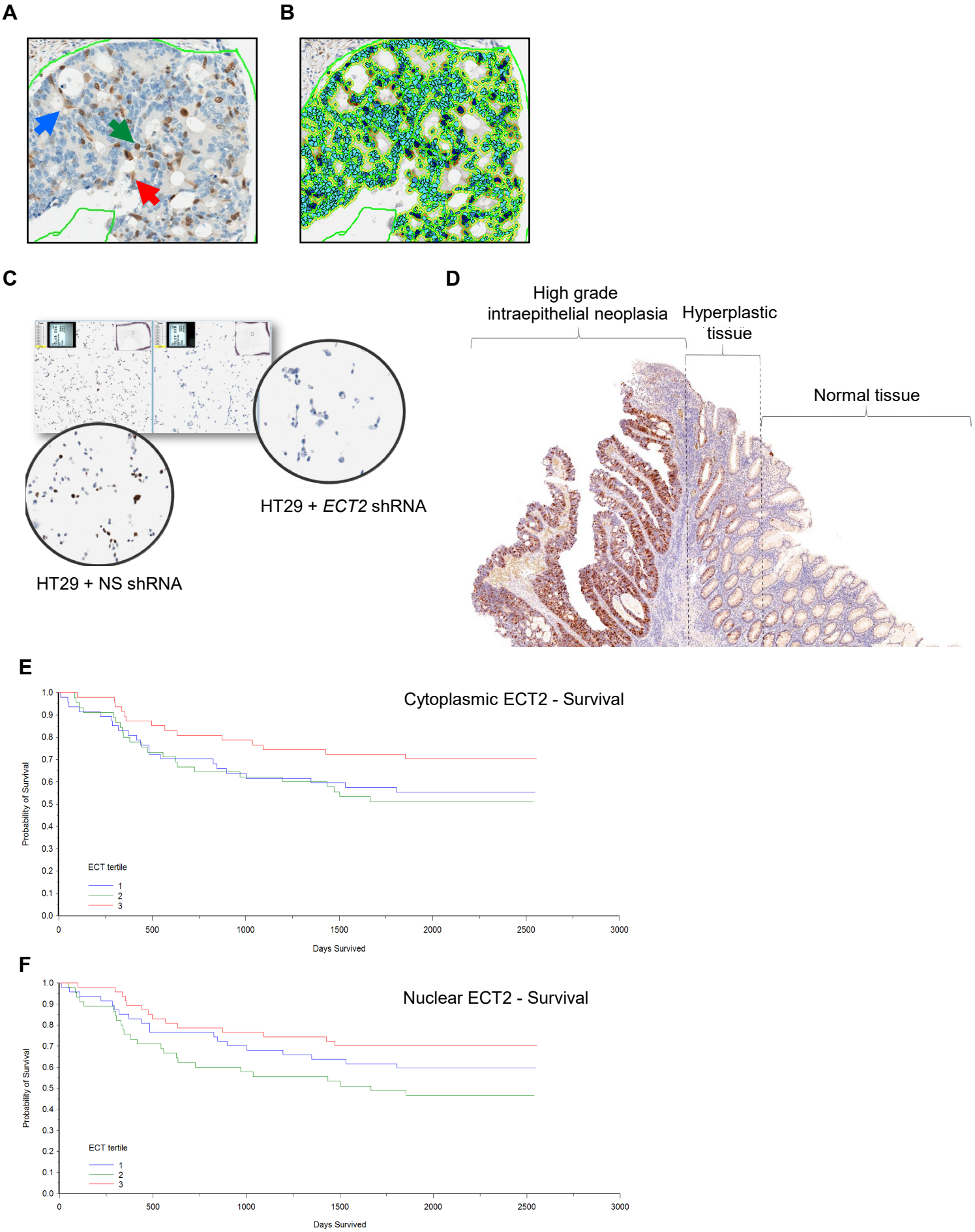

Supplementary Figure S2. Immunohistochemistry analyses of ECT2 expression which is associated with overall survival. **A-B**, Computational analyses of cytoplasmic and nuclear ECT2 immunohistochemistry (IHC) staining in CRC tumor tissue. Colorectal epithelium in tissue microarray (TMA) cores were circled manually (solid green line) to include it in analysis. Within the circled section, debris, stroma and non-epithelial cells were circled (dashed green line) to exclude these from analysis. In **A**, the red arrow denotes ECT2 in the cytoplasm, the green arrow denotes ECT2 stained in the nucleus, and the blue arrow points at a cell with both nuclear and cytoplasmic staining. After analysis, Aperio Imagescope obtained nuclear and cytoplasmic staining scores as shown in panel **B**. Light to medium to dark blue colors denote increasing nuclear staining intensities while yellow to orange to red colors denote increasing cytoplasmic staining intensities. **C**, Validation of the anti-ECT2 antibody in HT-29 cells, stably infected with non-targeted (NS) or *ECT2* shRNA #2, for IHC analyses. **D**, Increased cytoplasmic and nuclear ECT2 protein levels in early colorectal lesions compared to normal tissue. Shown is a representative IHC image for adjacent non-tumor colorectal tissue, hyperplastic and high-grade intraepithelial neoplasia with increasing intensity of ECT2 staining (40x magnification). **E, F,** Kaplan-Meier overall survival curve are shown for cytoplasmic (**E**) and nuclear ECT2 **(F**). No statistical differences based on log-rank test, see Table 1 for n.

Figure S3 Cook et al.

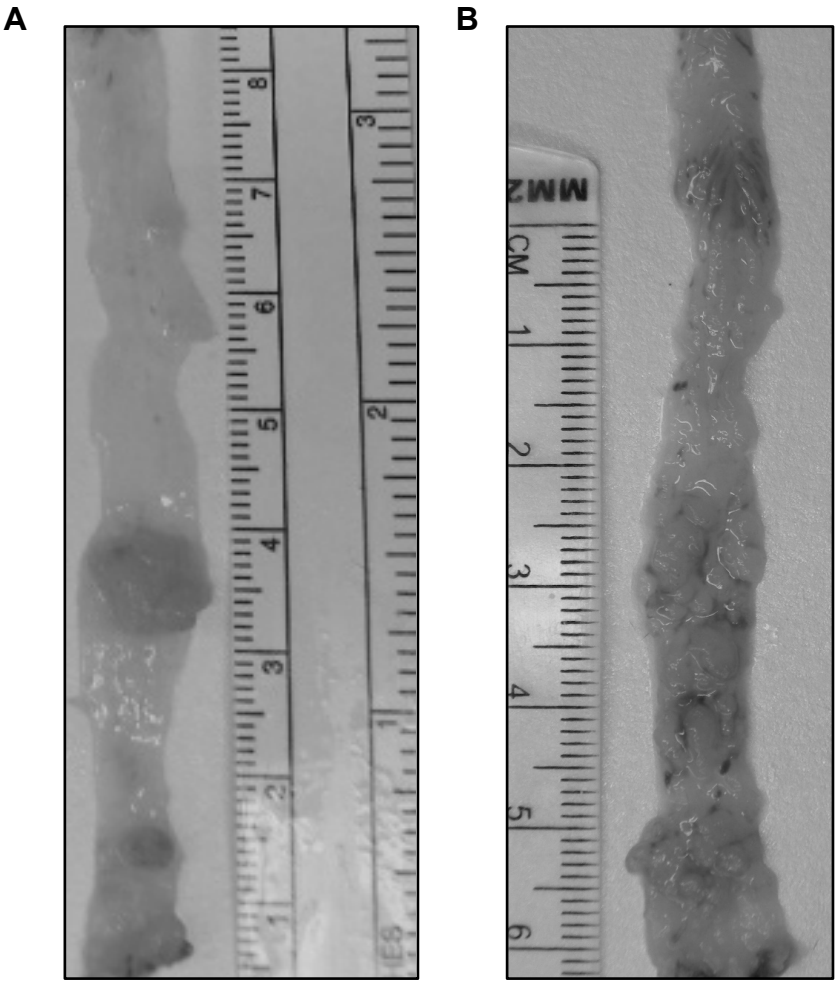

Fabpl-Cre; *Apc*$^{2lox14/+}$; *Kras*$^{LSL-G12D}$; *Ect2*$^{fl/fl}$

Fabpl-Cre; *Apc*$^{2lox14/+}$; *Kras*$^{LSL-G12D}$; *Ect2*$^{fl/+}$

Supplementary Figure S3. Representative gross images of intestines from (**A**) *Fabpl-Cre;Apc*$^{2lox14/+}$; *Kras*$^{LSL-G12D}$; *Ect2*$^{fl/fl}$ at 23.6 weeks compared to (**B**) *Fabpl-Cre;Apc*$^{2lox14/+;}$ *Kras*$^{LSL-G12D}$; *Ect2*$^{fl/+}$ at 7.1 weeks showing polyps carpeted throughout in the *Fabpl-Cre;Apc*$^{2lox14/+}$; *Kras*$^{LSL-G12D}$; *Ect2*$^{fl/+}$ mouse at a much earlier age which caused subsequent obstruction, compared to significantly fewer polyps in the *Fabpl-Cre*;*Apc*$^{2lox14/+}$; *Kras*$^{LSL-G12D}$; *Ect2*$^{fl/fl}$ mouse. Scale as indicated.

Figure S4 Cook et al.

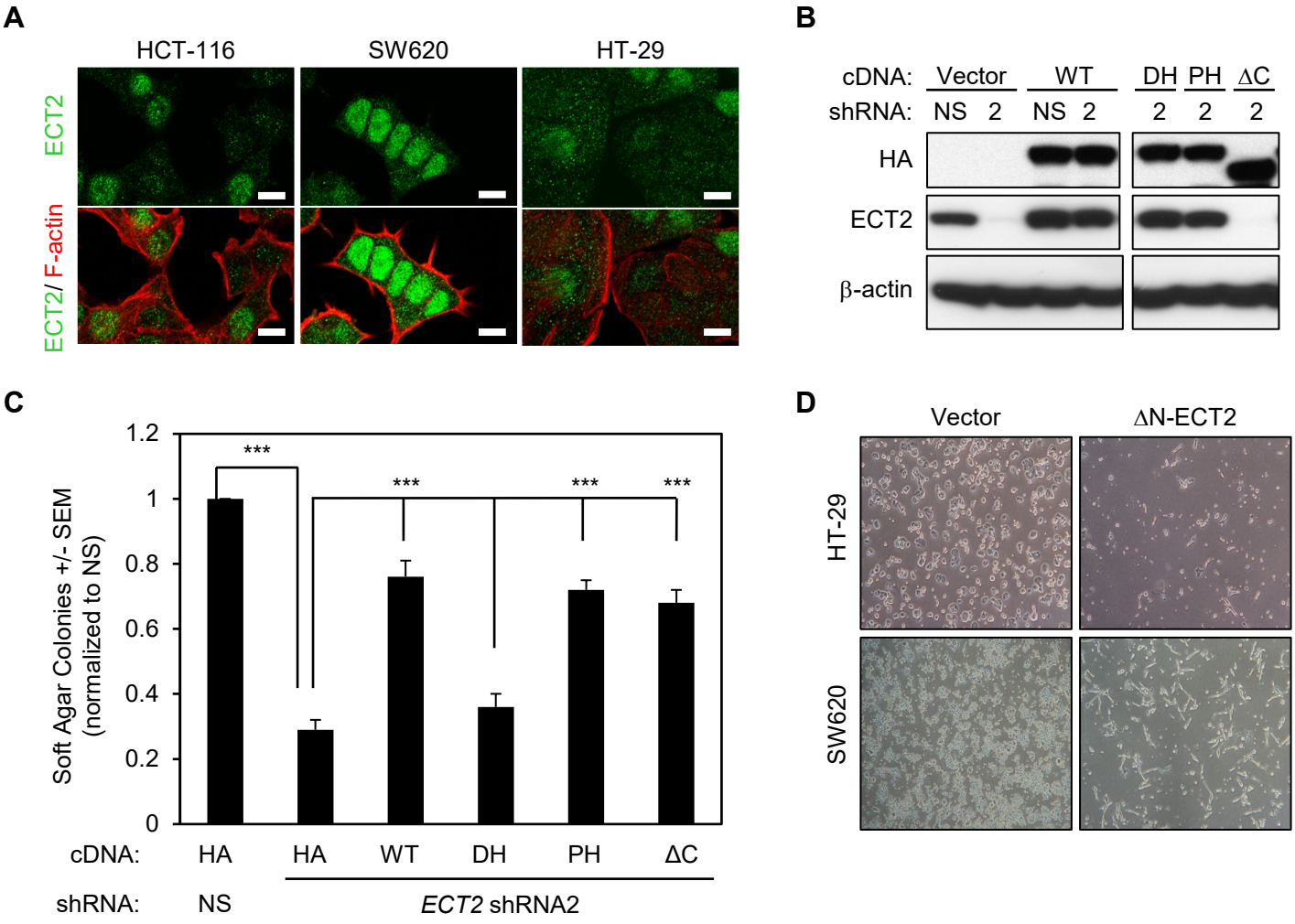

Supplementary Figure S4. Characterization of endogenous ECT2 and ectopically expressed ECT2 mutants in human CRC cell lines**. A**, Immunofluorescence microscopy analyses to determine subcellular localization of endogenous ECT2 (green) in indicated human CRC cell lines. F-actin (red) was used as control to visualize cell size and morphology. Images are representative of three independent experiments. Scale bar, 10 mm. **B**, Representative western blot analysis of HT-29 cells with stable suppression of endogenous ECT2 via shRNA #2 and ectopic expression of hemagglutinin (HA) epitope-tagged ECT2 mutants as indicated. **C**, Anchorage-independent growth (soft agar colony formation) normalized as a function of expression of indicated ectopically expressed ECT2 mutants upon depletion of endogenous ECT2 using shRNA #2 or, using control nonspecific shRNA (NS); Data are mean ± SD, n = 3, ***P<0.001, unpaired t-test. **D**, Representative phase-contrast images (10x magnification) to visualize the cell morphology of HT-29 and SW620 cells transiently infected with the control empty vector or encoding constitutively activated ΔN-ECT2.